Electronic Supplementary Information

Robust lanthanide MOFs as multifunctional luminescent sensors for intelligent visualization monitoring of MEAA and texture code anti-counterfeiting applications

Hui-Min Yang, Guo-Ping Yang *, and Yao-Yu Wang *

Key Laboratory of Synthetic and Natural Functional Molecule of the Ministry of Education, Shaanxi Key Laboratory of Physico-Inorganic Chemistry, Xi'an Key Laboratory of Functional Supramolecular Structure and Materials, College of Chemistry and Materials Science, Northwest University, Xi'an 710127, P.R. China

E-mail: ygp@nwu.edu.cn; wyaoyu@nwu.edu.cn.

Table of Contents

Supporting Fig.

Fig. S1	FT-IR spectrogram of **1-Eu** and **1-Tb**
Fig. S2	Coordination modes of L^{2-} in **1-Eu**
Fig. S3	The TGA curves of (a) **1-Eu** and (b) **1-Tb**
Fig. S4	PXRD patterns of simulated **1-Eu** and synthesized samples of **1-Eu** and **1-Tb**
Fig. S5	PXRD patterns of **1-Eu** water tolerability experiments
Fig. S6	The PXRD patterns of **1-Eu** in different pH conditions
Fig. S7	(a) Excitation and emission spectra of **H_2L**
Fig. S8	(a) Excitation and (b) emission spectra of **1-Eu**
Fig. S9	The CIE coordinates of (a) **1-Eu** and (b) **1-Tb**
Fig. S10	(a) Excitation and (b) emission spectra of **1-Tb**
Fig. S11	Schematic diagram of the energy absorption, transfer and emission processes of **1-Eu** and **1-Tb**
Fig. S12	Emission spectra of **1-Eu** before and after soaking in deionized water for 7 days
Fig. S13	Emission intensity of **1-Eu** at different (a) pH and (b) solvents
Fig. S14	PXRD patterns of a series of bimetallic MOFs **1-Eu_xTb_{1-x}**
Fig. S15	Luminescent decay curves of (a) **1-Eu** and (b) **1-Tb**
Fig. S16	Schematic diagram of energy transfer processes in 1-**Eu_xTb_{1-x}**
Fig. S17	Different components were added to simulate the relative fluorescence intensity of **1-Eu** in (a) urine and (b) blood
Fig. S18	Fluorescence responses of **1-Eu** in the presence of various (a) urine and (b) blood substances before and after adding MEAA
Fig. S19	Relative fluorescence intensity and sensing ability(MEAA) of **1-Eu** suspensions in different solvents
Fig. S20	Relative fluorescence intensity and sensing ability(MEAA) of **1-Eu** suspensions in different alcohols
Fig. S21	SEM images of **1-Eu** (a) before and (b) after 6 cycles
Fig. S22	PXRD patterns of **1-Eu** before and after 6 cycles
Fig. S23	XPS images of **1-Eu** before and after adding MEAA
Fig. S24	Histogram of MEAA concentration to **1-Eu** emission intensity ratios
Fig. S25	UV-vis absorption spectra of MEAA and the excitation and emission spectra of **1-Eu**
Fig. S26	Schematic diagram of PET energy transfer processes.
Fig. S27	Luminescence lifetime patterns of **1-Eu** suspensions with the presence of MEAA of different concentrations.

Supporting Tables

Table S1	Crystallographic Data of **1-Eu** and **1-Tb**
Table S2	Selected bond lengths (Å) and bond angles (°) for **1-Eu** and **1-Tb**
Table S3	Comparison chemical and thermal stability conditions of selected stable MOFs
Table S4	ICP-AES results of a series of bimetallic-doped **1-Eu_xTb_{1-x}**
Table S5	Photoluminescence data of **1-Ln** and **1-Eu_xTb_{1-x}**
Table S6	HOMO and LUMO Energies for H_2L and MEAA
Table S7	The hexadecimal color codes of each color block of QR code

Section S1 Materials, Characterization and Synthesis Methods.

All the reagents and solvents were purchased to use without further purification in the experiments. Infrared spectra were examined on Bruker EQUINOX-55 spectrophotometer in 4000–400 cm^{-1} (KBr pellets). Powder X-ray diffraction patterns were investigated through Bruker D8 ADVANCE X-ray powder diffractometer. Thermogravimetric analyses were tested on NETZSCH STA 449C microanalyzer (N_2 atmosphere, 10 °C min^{-1}). UV-vis spectra were measured on Hitachi U-3310 spectrometer. Luminescent spectra and luminescence lifetimes were determined on an Edinburgh FLS920 fluorescence spectrometer. The quantum efficiency was tested by an integrating sphere on a FluoroMax-4 spectrophotometer. The bimetallic doping molar ratio was determined by inductively coupled plasma mass spectrometry (ICP-MS) Agilent 7900. X-ray photoelectron spectroscopy (XPS) was carried out on the UIVAC-PHI 5000 Versa Probe with Al target as the excitation source.

Section S2 X-ray Crystal Structure Determination.

The single-crystal X-ray diffractions were tested on Bruker SMART APEX II CCD diffractometer equipped with graphite monochromated Mo Kα radiation (λ = 0.71073Å) *via* ϕ/ω scan method. The diffraction data were corrected for Lorentz and polarization effects for empirical absorption based on multiscan. The structures were solved by the direct methods and refined on F^2 *via SHELXTL* program.[18] The anisotropic thermal parameters were applied to non-hydrogen atoms. The hydrogen atoms of ligands were calculated and added at ideal positions. Table S1 and Table S2 summarized X-ray crystallographic data and refinement details for **1-Eu** and **1-Tb**. The CCDC reference numbers were 2308030 and 2308031 for **1-Eu** and **1-Tb**.

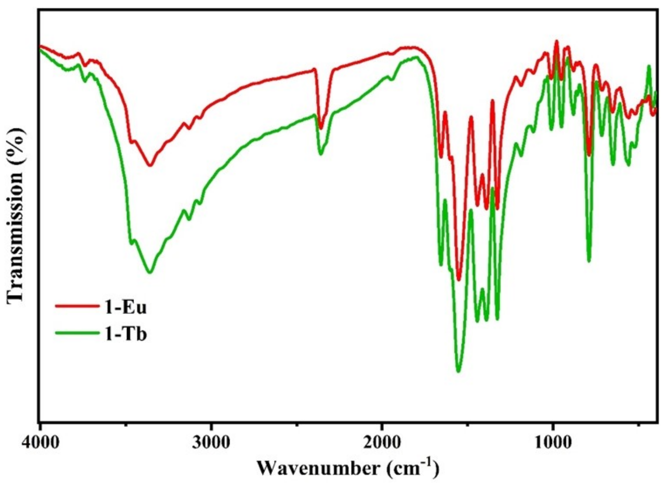

Fig. S1. FT-IR spectrogram of **1-Eu** and **1-Tb**.

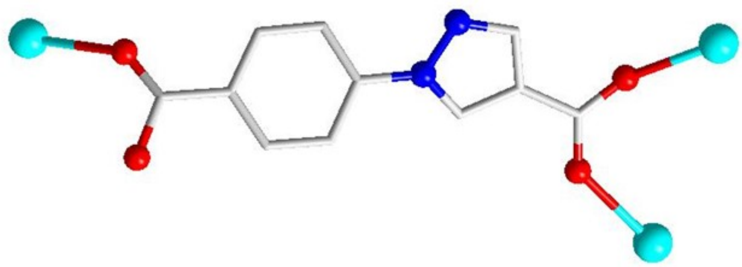

Fig. S2. Coordination modes of L^{2-} in **1-Eu**.

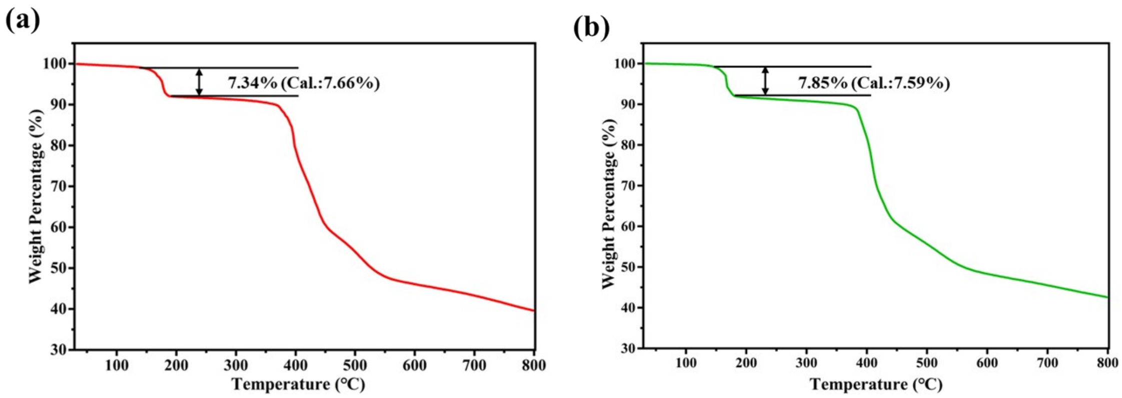

Fig. S3. The thermogravimetric (TGA) curves of (a) **1-Eu** and (b) **1-Tb** under N_2 environment.

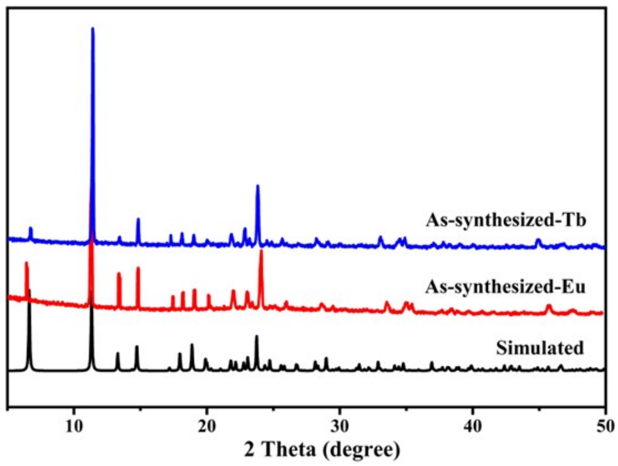

Fig. S4. PXRD patterns of **1-Eu** simulated from the X-ray single-crystal structure and as-synthesized samples of **1-Eu** and **1-Tb**.

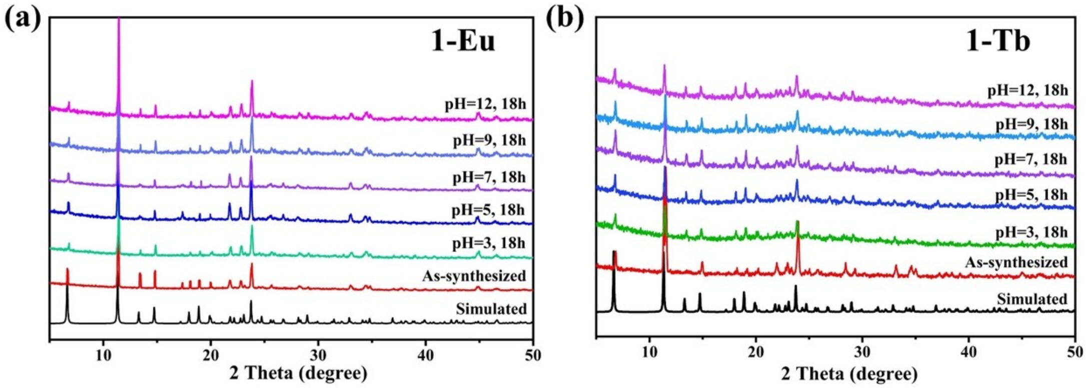

Fig. S5. PXRD patterns in different pH: (a) **1-Eu**; (b) **1-Tb**.

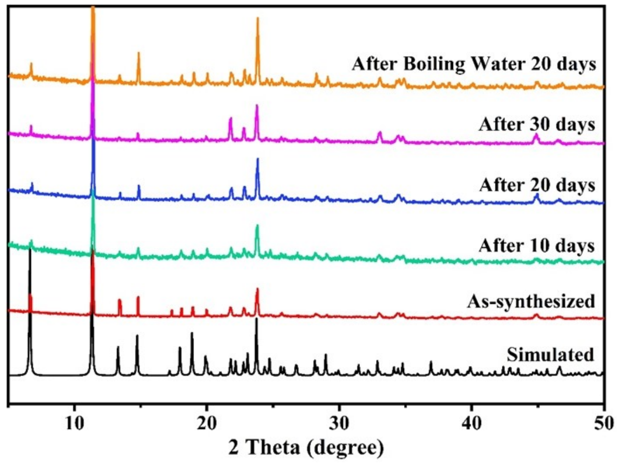

Fig. S6. PXRD patterns of **1-Eu** water tolerability experiments.

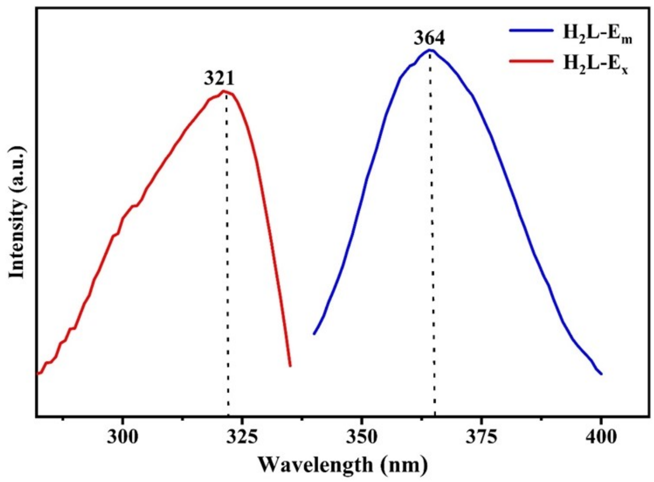

Fig. S7. (a) Excitation and emission spectra of $\mathbf{H_2L}$ (λ_{ex} =321 nm).

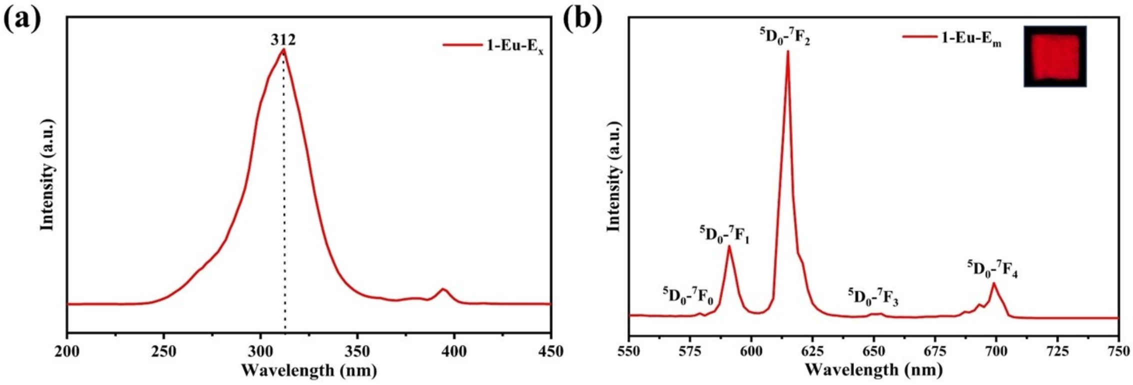

Fig. S8. (a) Excitation and (b) emission spectra of **1-Eu** (Inset, the image of **1-Eu** under the irradiation at 254 nm).

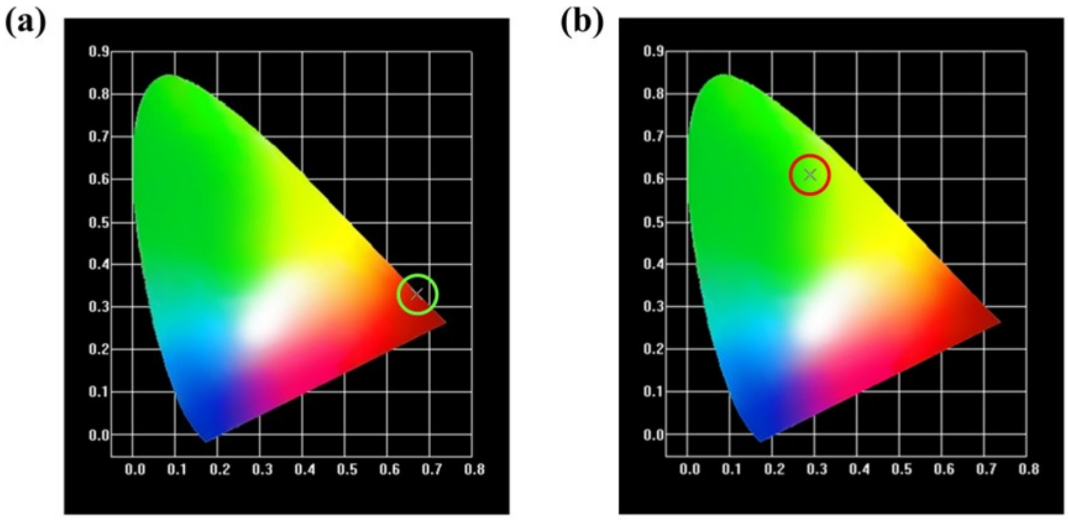

Fig. S9. CIE coordinates of (a) **1-Eu** and (b) **1-Tb**.

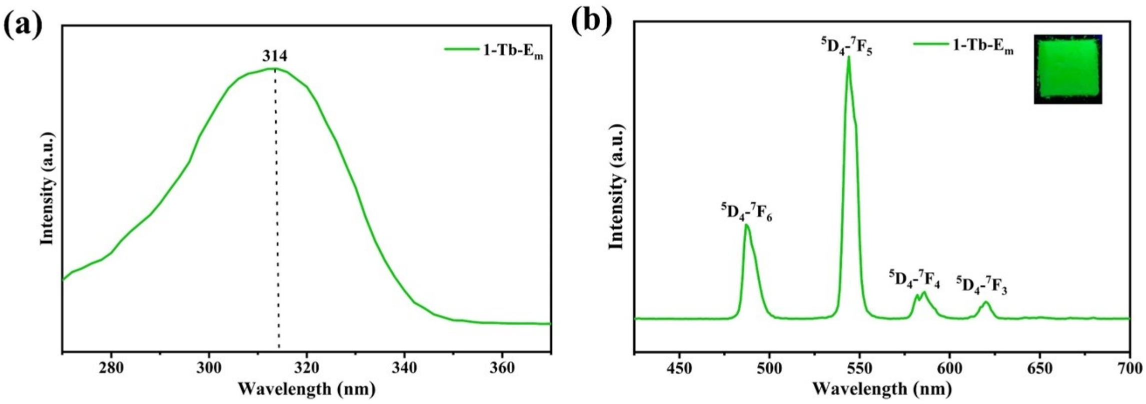

Fig. S10. (a) Excitation and (b) emission spectra of **1-Tb** (Inset, the image of **1-Tb** under the irradiation at 254 nm).

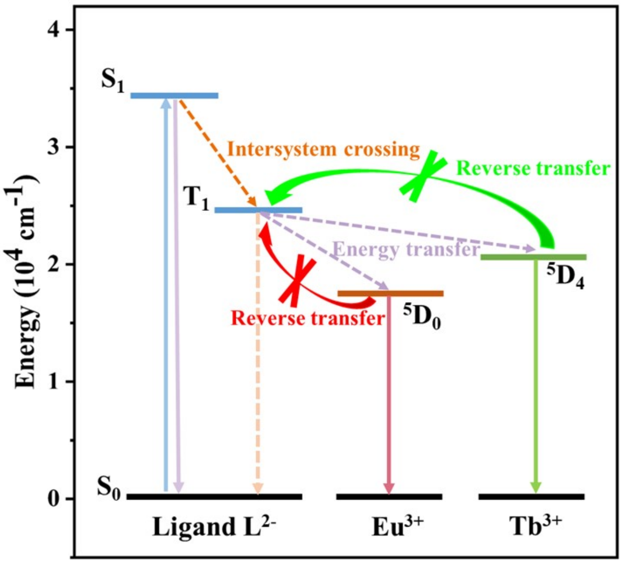

Fig. S11. Schematic diagram of the energy absorption, transfer and emission processes of **1-Eu** and **1-Tb**.

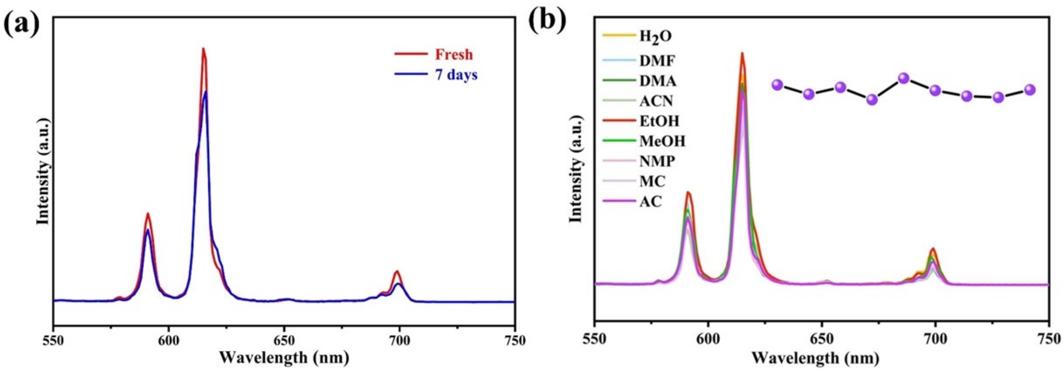

Fig. S12. Emission spectra of **1-Eu** (a) before and after soaking in deionized water for 7 days; (b) in different solvents.

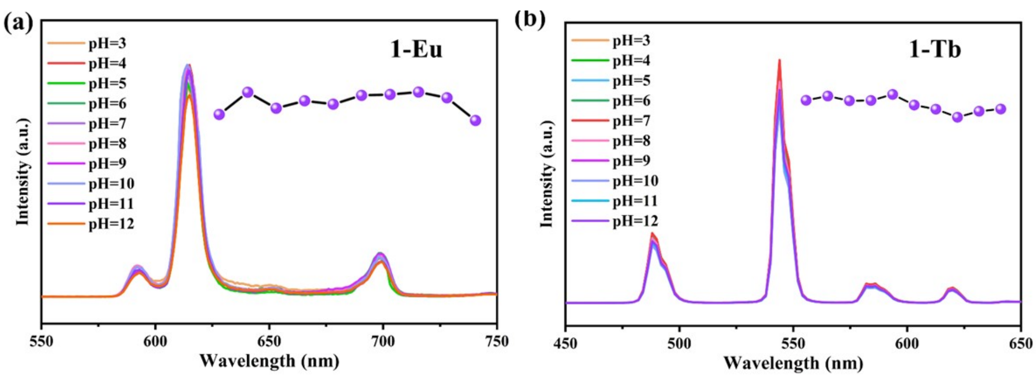

Fig. S13. Emission intensity in different pH of (a) **1-Eu**; (b) **1-Tb**.

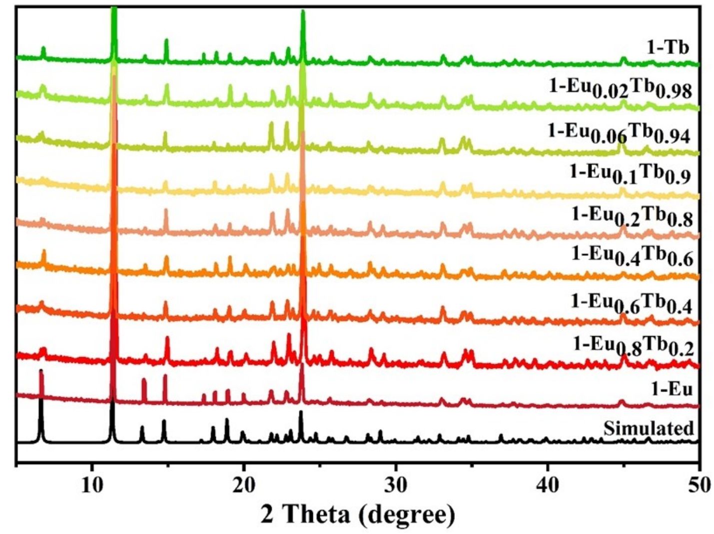

Fig. S14. PXRD patterns for a series of MOFs **1-Eu$_x$Tb$_{1-x}$**.

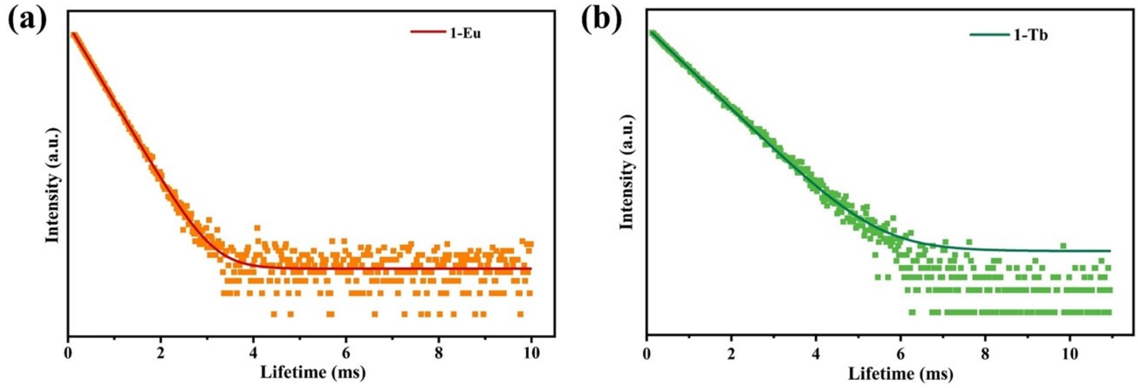

Fig. S15. Luminescent decay curves of (a) **1-Eu** and (b) **1-Tb**.

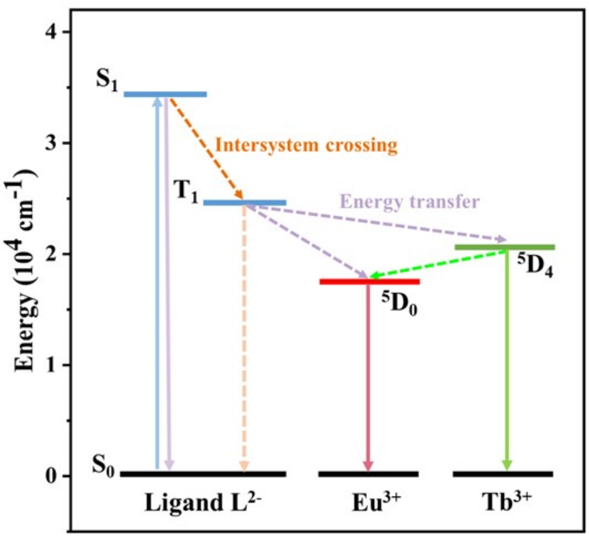

Fig. S16. Schematic diagram of energy transfer processes in **1-Eu$_x$Tb$_{1-x}$**.

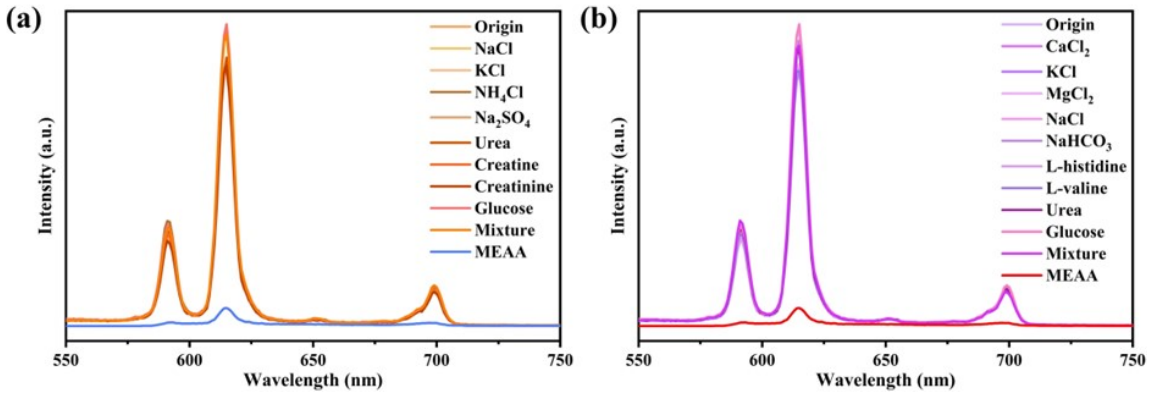

Fig. S17. Different components were added to simulate the relative fluorescence intensity of **1-Eu** in (a) urine and (b) blood.

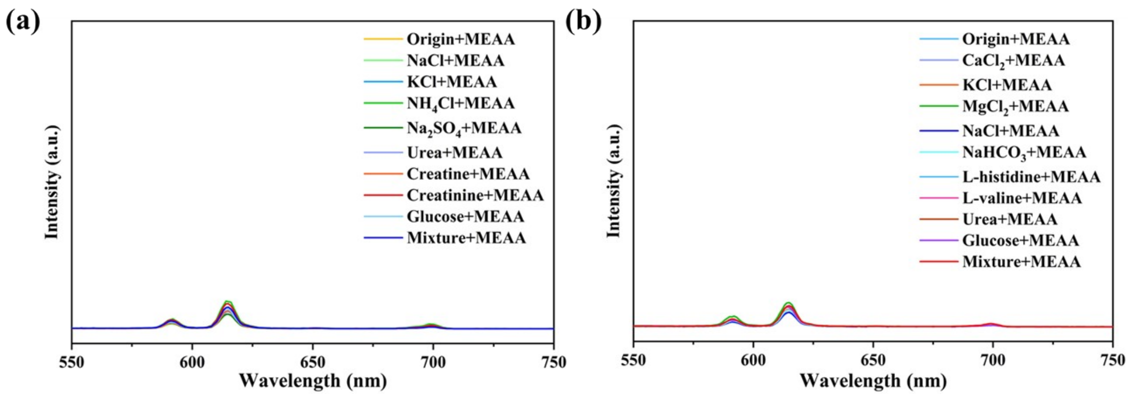

Fig. S18. Fluorescence responses of **1-Eu** in the presence of various (a) urine and (b) blood substances before and after adding MEAA.

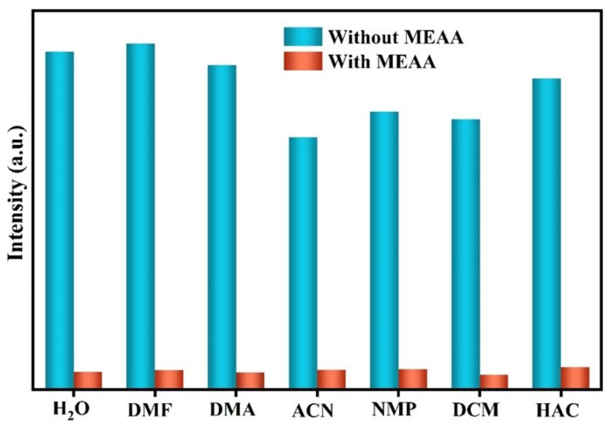

Fig. S19. Relative fluorescence intensity and sensing ability(MEAA) of **1-Eu** suspensions in different solvents (DMF: N,N-Dimethylformamide ; DMA: N,N- Dimethylacetamide; ACN: Acetonitrile; NMP:1-Methyl-2-pyrrolidinone; DCM: Dichloromethane; HAC:acetic acid).

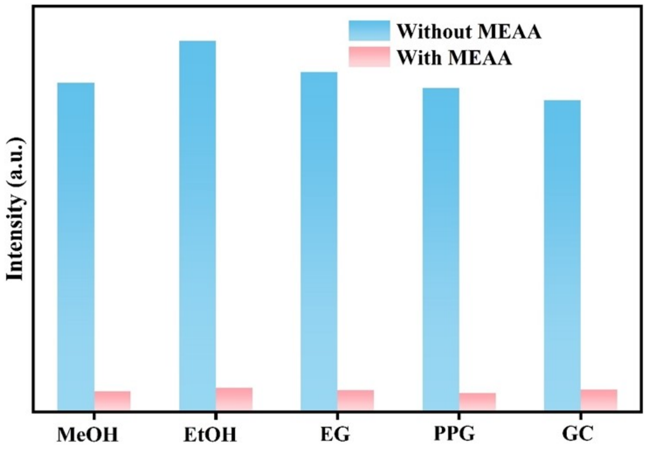

Fig. S20. Relative fluorescence intensity and sensing ability(MEAA) of **1-Eu** suspensions in different alcohols(MeOH: methanol; EtOH: ethanol; EG: ethylene glycol; PPG: propylene glycol; GC: glycerin).

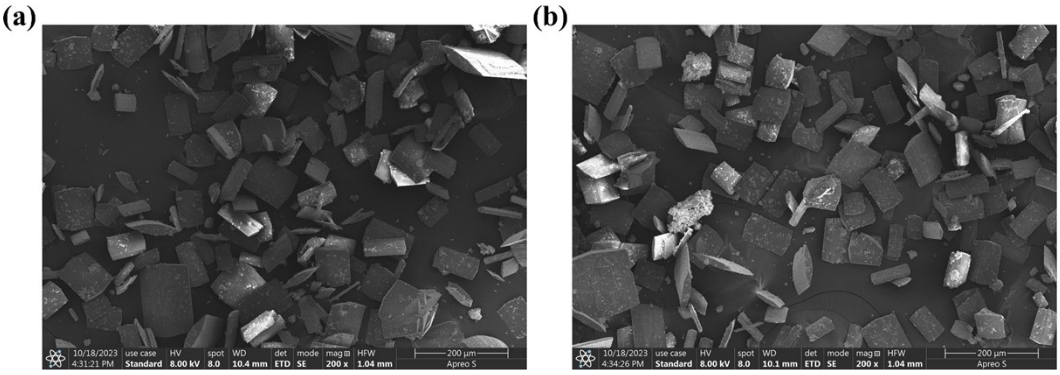

Fig. S21. The SEM images of **1-Eu** (a) before and (b) after 6 cycles.

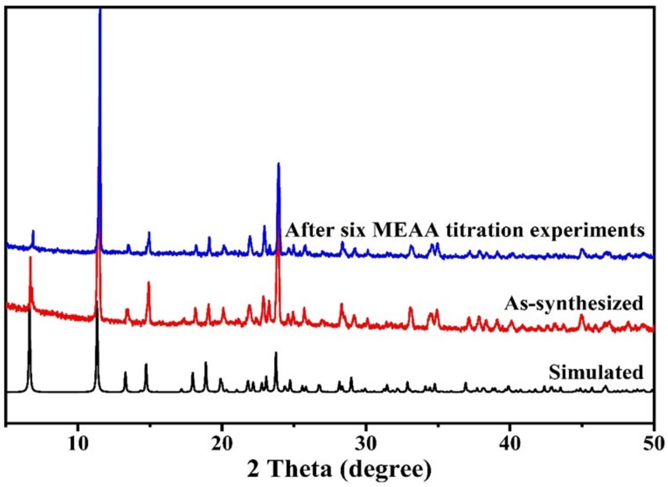

Fig. S22. PXRD patterns of **1-Eu** before and after 6 cycles.

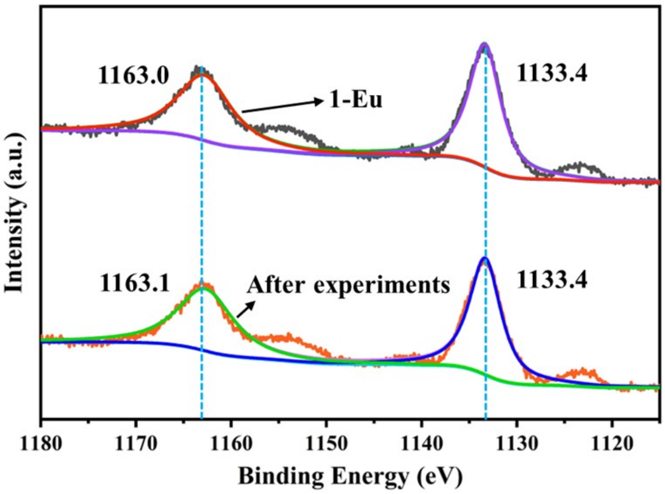

Fig. S23. XPS images of **1-Eu** before and after adding MEAA.

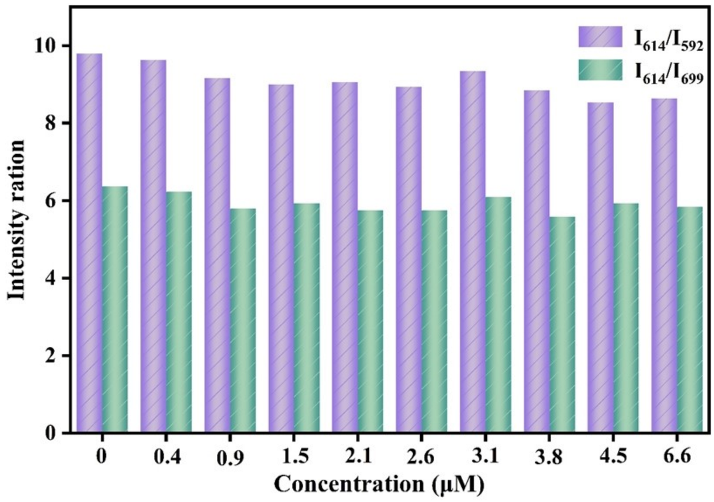

Fig. S24. Histogram of MEAA concentration to **1-Eu** emission intensity ratios.

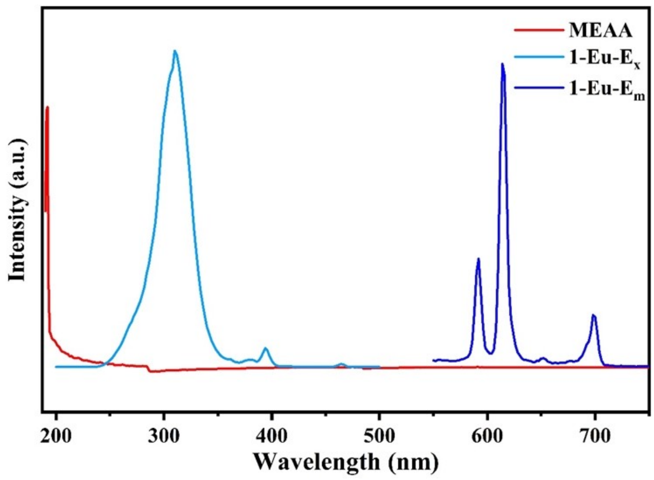

Fig. S25. UV-vis absorption spectra of MEAA and the excitation and emission spectra of **1-Eu**.

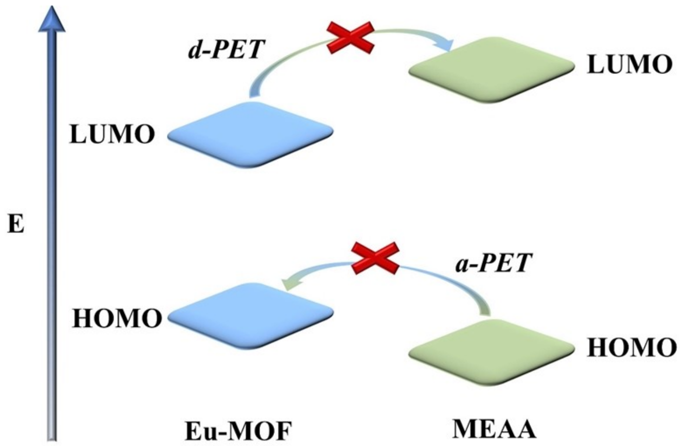

Fig. S26. Schematic diagram of PET energy transfer processes.

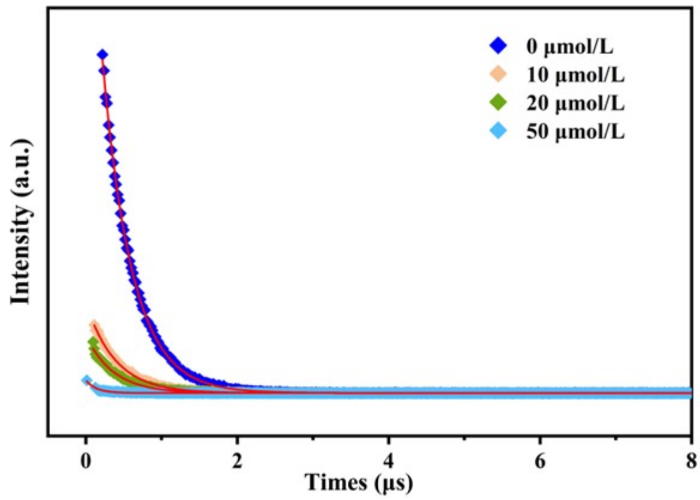

Fig. S27. Luminescence lifetime patterns of $^{5}D_0$ in **1-Eu** suspensions with the presence of MEAA of different concentrations.

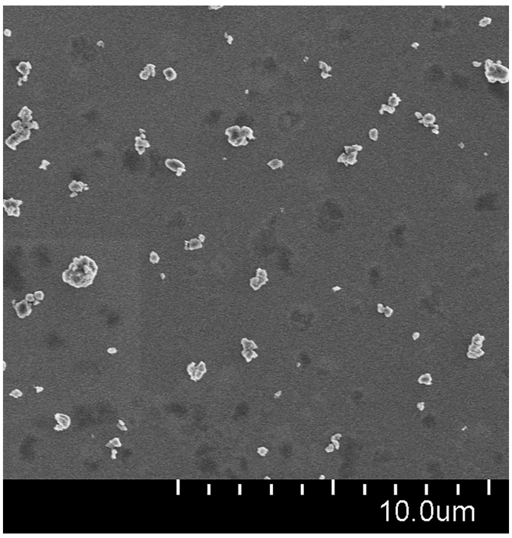

Fig. S28. SEM image of **1-Ln** after grinding.

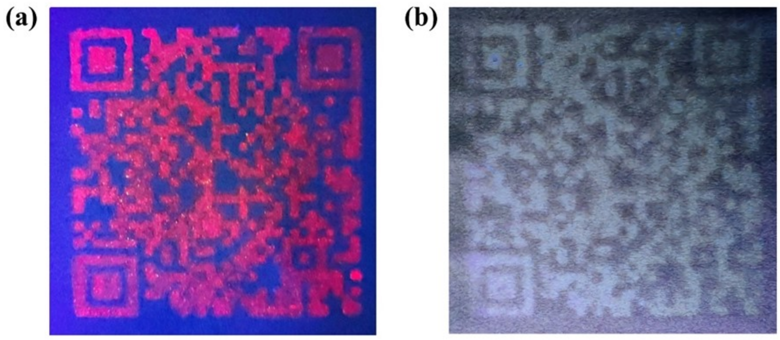

Fig. S29. QR code in different conditions after (a) six months; (b) the luminescent quenching of MEAA.

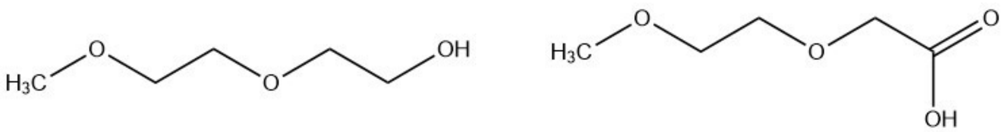

Scheme S1. Structures of 2-(2-methoxyethoxy)ethanol and 2-(2-methoxyethoxy)acetic acid .

Table S1. Crystallographic data of **1-Eu** and **1-Tb**.

complex	1-Eu	1-Tb
empirical formula	$Eu_{0.5}C_{11}H_9N_2O_5$	$Tb_{0.5}C_{11}H_9N_2O_5$
formula mass	325.18	328.66
crystal system	Orthorhombic	Orthorhombic
space group	*Pccn*	*Pccn*
a [Å]	26.6183(13)	26.5851(16)
b [Å]	8.1659(4)	8.1405(5)
c [Å]	10.0386(5)	10.0208(6)
α [°]	90	90
β [°]	90	90
γ [°]	90	90
V [Å^3]	2182.01(19)	2168.7(2)
Z	8	8
ρ_{calcd} [g cm^{-3}]	1.980	2.013
μ [mm^{-1}]	2.945	3.332
F [000]	1284	1292
θ [°]	3.061-25.444	3.314 -25.345
reflections collected	10355	15503
goodness-of-fit on F^2	1.003	1.200
$R_1{}^a$ [$I > 2\sigma(I)$]	0.0343	0.0259
$wR_2{}^b$ (all data)	0.0771	0.0537

$^aR_1 = \sum||F_o| - |F_c||/\sum|F_o|$. $^bwR_2 = [\sum w(F_o{}^2 - F_c{}^2)^2/\sum w(F_o{}^2)^2]^{1/2}$

Table S2. Selected bond lengths (Å) and bond angles (°) for **1-Eu** and **1-Tb**.

1-Eu			
Eu(1)-O(1)#1	2.321(3)	O(3)#3-Eu(1)-O(3)	118.38(17)
Eu(1)-O(1)#2	2.321(3)	O(3)-Eu(1)-O(4)#5	73.97(12)
Eu(1)-O(3)	2.454(4)	O(3)#3-Eu(1)-O(4)#5	134.40(11)
Eu(1)-O(3)#3	2.454(4)	O(3)#3-Eu(1)-O(4)#4	73.97(12)
Eu(1)-O(4)#4	2.513(3)	O(3)-Eu(1)-O(4)#4	134.40(11)
Eu(1)-O(4)#5	2.513(3)	O(4)#4-Eu(1)-O(4)#5	131.16(15)
Eu(1)-O(5)#3	2.405(3)	O(5)-Eu(1)-O(3)#3	70.99(12)
Eu(1)-O(5)	2.405(3)	O(5)#3-Eu(1)-O(3)	70.99(12)
O(1)#1-Eu(1)-O(1)#2	90.53(18)	O(5)#3-Eu(1)-O(3)#3	76.35(12)
O(1)#2-Eu(1)-O(3)#3	82.78(13)	O(5)-Eu(1)-O(3)	76.35(12)
O(1)#1-Eu(1)-O(3)	82.78(13)	O(5)-Eu(1)-O(4)#4	142.27(12)
O(1)#1-Eu(1)-O(3)#3	147.85(12)	O(5)-Eu(1)-O(4)#5	70.28(11)
O(1)#2-Eu(1)-O(3)	147.85(12)	O(5)#3-Eu(1)-O(4)#5	142.27(12)
O(1)#1-Eu(1)-O(4)#5	72.11(8)	O(5)#3-Eu(1)-O(4)#4	70.28(11)
O(1)#2-Eu(1)-O(4)#4	72.11(8)	O(5)#3-Eu(1)-O(5)	113.48(17)
O(1)#1-Eu(1)-O(4)#4	74.05(12)	C(10)-O(1)-Eu(1)#6	147.2(3)
O(1)#2-Eu(1)-O(4)#5	74.05(12)	Eu(1)-O(3)-H(3A)	109.3
O(1)#2-Eu(1)-O(5)#3	140.69(12)	Eu(1)-O(3)-H(3B)	110.0
O(1)#1-Eu(1)-O(5)#3	89.90(11)	C(5)-O(4)-Eu(1)#5	134.9(4)
O(1)#1-Eu(1)-O(5)	140.69(12)	C(10)-O(5)-Eu(1)	136.8(3)
O(1)#2-Eu(1)-O(5)	89.90(11)		
1-Tb			
Tb(1)-O(1)	2.445(3)	O(4)#4-Tb(1)-O(4)#5	130.83(13
Tb(1)-O(1)#1	2.445(3)	O(5)-Tb(1)-O(1)#1	148.19(10)
Tb(1)-O(3)#2	2.390(3)	O(5)#1-Tb(1)-O(1)#1	82.73(10)
Tb(1)-O(3)#3	2.390(3)	O(5)-Tb(1)-O(1)	82.72(10)
Tb(1)-O(4)#4	2.491(3)	O(5)-Tb(1)-O(3)#2	140.48(10)
Tb(1)-O(4)#5	2.491(3)	O(5)#1-Tb(1)-O(3)#3	140.48(10)
Tb(1)-O(5)#1	2.296(3)	O(5)#1-Tb(1)-O(3)#2	90.39(10)
Tb(1)-O(5)	2.296(3)	O(5)-Tb(1)-O(3)#3	90.39(10)
Tb(1)-O(1)	2.445(3)	O(5)-Tb(1)-O(4)#4	74.36(10)
O(1)#1-Tb(1)-O(1)	118.35(14)	O(5)#1-Tb(1)-O(4)#5	74.36(10)
O(1)#1-Tb(1)-O(4)#5	134.61(9)	O(5)-Tb(1)-O(4)#5	71.48(9)
O(1)-Tb(1)-O(4)#5	73.99(10)	O(5)#1-Tb(1)-O(4)#4	71.48(9)
O(1)#1-Tb(1)-O(4)#4	73.98(10)	O(5)-Tb(1)-O(5)#1	90.24(14)

O(1)-Tb(1)-O(4)#4	134.61(9)	Tb(1)-O(1)-H(1A)	109.2
O(3)#3-Tb(1)-O(1)#1	76.29(10)	Tb(1)-O(1)-H(1B)	109.3
O(3)#2-Tb(1)-O(1)#1	70.84(10)	O(5)-Tb(1)-O(1)#1	148.19(10)
O(3)#3-Tb(1)-O(1)	70.84(10)	O(5)#1-Tb(1)-O(1)#1	82.73(10)
O(3)#2-Tb(1)-O(1)	76.29(10)	O(5)-Tb(1)-O(1)	82.72(10)
O(3)#2-Tb(1)-O(3)#3	113.06(14)	O(5)-Tb(1)-O(3)#2	140.48(10)
O(3)#2-Tb(1)-O(4)#5	70.71(9)	C(3)-O(3)-Tb(1)#6	137.0(2)
O(3)#3-Tb(1)-O(4)#5	142.12(10)	C(9)-O(4)-Tb(1)#7	134.8(3)
O(3)#3-Tb(1)-O(4)#4	70.71(9)	C(3)-O(5)-Tb(1)	146.9(3)
O(3)#2-Tb(1)-O(4)#4	142.12(10)		

Symmetry transformations used to generate equivalent atoms:

1-Eu: #1 -x+3/2, y, z+1/2; #2 x, -y+3/2, z+1/2; #3 -x+3/2, -y+3/2, z; #4 x+1/2, y+1/2, -z+1; #5 -x+1, -y+1, -z+1; #6 x, -y+3/2, z-1/2. **1-Tb**: #1 -x+1/2, -y+3/2, z; #2 -x+1/2, y, z-1/2; #3 x, -y+3/2, z-1/2; #4 -x+1, y+1/2, -z+3/2; #5 x-1/2, -y+1, -z+3/2; #6 x, -y+3/2, z+1/2; #7 -x+1, y-1/2, -z+3/2.

Table S3. Comparison chemical and thermal stability conditions of selected stable MOFs.

MOFs	Chemical stability	Thermal stability (°C)	Ref.
1-Eu	pH = 3-12 for 12 h, water for 30 days, boiling water for 20 days	375	This work
NIIC1-Ln	pH = 2-12 for 3 h, Water for 5 days, boiling water for 7 days	450	1
LCP	pH = 2-10 for 12 h, organic and Water for 12 h	-	2
CMERI-1&2	Soaked in HCl(PH = 3) and NaOH(4 M)	286 & 350	3
B-EuMOF	pH = 4-8, Water for 48 h	400	4
$[Cd_3(BDC)_3(DMF)_2]$	——	310	5
BCD@EuBTC	——	370	6
NOTT-220	pH = 2-12 and water for 7 days	390	7
S-1	pH = 4-12 for 4 h, organic solvents for 10 h, water and boiling water for 10 weeks	310	8
PCN-601	0.1 mM HCl, 10 M NaOH (100 °C) for 1day	500	9
FJU-99	Some organic solvents	200	10

Table S4. ICP-AES results of a series of bimetallic-doped **1-Eu$_x$Tb$_{1-x}$**.

Compound	Eu content in mol (%)	Tb content in mol (%)
1-Eu$_{0.02}$Tb$_{0.98}$	2.3	97.7
1-Eu$_{0.06}$Tb$_{0.94}$	6.2	93.8
1-Eu$_{0.1}$Tb$_{0.9}$	9.5	90.5
1-Eu$_{0.2}$Tb$_{0.8}$	20.4	79.6
1-Eu$_{0.4}$Tb$_{0.6}$	39.9	60.1
1-Eu$_{0.6}$Tb$_{0.4}$	60.6	39.4
1-Eu$_{0.8}$Tb$_{0.2}$	79.8	20.2

Table S5. Photoluminescence data of **1-Ln** and **1-Eu$_x$Tb$_{1-x}$**.

Compounds	CIE coordinates	τ (μs)	η (%)
1-Tb	(0.29,0.61)	816.62	——
1-Eu$_{0.02}$Tb$_{0.98}$	(0.33,0.57)	731.37	11.04
1-Eu$_{0.06}$Tb$_{0.94}$	(0.35,0.55)	690.03	15.51
1-Eu$_{0.1}$Tb$_{0.98}$	(0.38,0.53)	612.38	25.11
1-Eu$_{0.2}$Tb$_{0.8}$	(0.49,0.45)	589.42	27.83
1-Eu$_{0.4}$Tb$_{0.6}$	(0.56,0.39)	443.82	45.66
1-Eu$_{0.6}$Tb$_{0.4}$	(0.58,0.37)	399.23	51.12
1-Eu$_{0.8}$Tb$_{0.2}$	(1.63,0.34)	387.78	52.53
1-Eu	(0.67,0.33)	387.73	——

Table S6. HOMO and LUMO Energies for H_2L and MEAA.

Analytes	HOMU (eV)	LUMO (eV)	Band Gap (eV)
H_2L	-6.803	-1.891	4.912
MEAA	-7.151	-0.016	7.135

Table S7. The hexadecimal color codes of each color block of QR code.

Eu					
27%	#455900	#45FF00	#451A00	#451200	
100%	#FF5900	#FFFF00	#FF1A00	#FF1200	
2%	#055900	#05FF00	#051A00	#051200	
13%	#215900	#21FF00	#211A00	#211200	
	35%	100%	10%	7%	Tb

Tb					
35%	#455900	#FF5900	#055900	#215900	
100%	#45FF00	#FFFF00	#05FF00	#21FF00	
10%	#451A00	#FF1A00	#051A00	#211A00	
7%	#451200	#FF1200	#051200	#211200	
	27%	100%	2%	13%	Eu

Eu					
27%	#450000	#A20000	#250000	#330000	
100%	#A20000	#FF0000	#820000	#900000	
2%	#250000	#820000	#050000	#130000	
13%	#330000	#900000	#130000	#210000	
	27%	100%	2%	13%	Eu

Tb					
35%	#005900	#00AC00	#003900	#003500	
100%	#00AC00	#00FF00	#008C00	#008800	
10%	#003900	#008C00	#001900	#001500	
7%	#003500	#008800	#001500	#001200	
	35%	100%	10%	7%	Tb

References

[1] Y. N. Zhou, L. L. Liu, Q. W. Liu, X. X. Liu, M. Z. Feng, L. Wang, Z. G. Sun, and Y. Y. Zhu, *Angew. Chem. Int. Ed.*, 2023, **62**, e202306680.

[2] Y. Wang, N. Xu, J. Ma, H. Li, Y. Zhang, G. Liu, and X. Wang, *Inorg. Chem.*, 2022, **61**, 7780−7786.

[3] S. Bej, S. Mandal, A. Mondal, T.K. Pal, and P. Banerjee, *ACS Appl. Mater. Interfaces.*, 2021,

13, 25153-25163.

[4] Y. Zhang, H. Lu, and B. Yan, *Sens. Actuator B-Chem.*, 2021, **349**, 130736.

[5] Y. F. Zhong, G. M. Bao, M. Qiu, Y. F. Xia, W. Li, Y. Q. Tao, S. Y. Liu, S. H. Li, W. Xiao, Y. Zhang, and H. Q. Yuan, *J. Mater. Chem. A.*, 2017, **5**, 15797- 15807.

[6] Y. Fei, K. Sun, and L. Liu, *pectrochim. Acta A Mol. Biomol. Spectrosc.*, 2023, **290**, 122244.

[7] L. Song, F. Tian, and Z. Liu, J. *Solid State Chem.*, 2022, **312**, 123231.

[8] T. Q. Song, K. Yuan, W. Z. Qiao, Y. Shi, J. Dong, H. L. Gao, X. P. Yang, J. Z. Cui, B. Zhao, *Anal. Chem.*, 2019, **91**, 2595-2599.

[9] K. Wang, X. L. Lv, D. Feng, J. Li, S. Chen, J. Sun, L. Song, Y. Xie, J. R. Li, and H. C. Zhou, *J. Am. Chem. Soc.*, 2016, **138**, 914-919.

[10] T. Chen, Y. Ye, M. Yin, L. Chen, Z. Ke, J. Guo, M. Zhang, Z. Yao, Z. Zhang, and S. Xiang, *Cryst. Growth Des.*, 2020, **20**, 2099-2105.